Journal of Magnetism and Magnetic Materials 513 (2020) 167164

Contents lists available at ScienceDirect

Journal of Magnetism and Magnetic Materials

journal homepage: www.elsevier.com/locate/jmmm

Analytic calculation for the stray field above Néel and Bloch magnetic domain walls in a rectangular nanoribbon

Carla Quispe Flores[a], Alexandra R. Stuart[b], Kristen S. Buchanan[a], Karen L. Livesey[b,*]

[a] Department of Physics, Colorado State University, Fort Collins, CO 80523, USA
[b] UCCS Biofrontiers Center and Department of Physics and Energy Science, University of Colorado Colorado Springs, 1420 Austin Bluffs Pkwy, Colorado Springs, CO 80918, USA

ARTICLE INFO

Keywords:
Magnetic nanowires
Domain walls
Analytic calculation
Micromagnetics

ABSTRACT

Narrow magnetic domain walls in rectangular nanowires with perpendicular anisotropy are a vital component for many spintronic devices. Probing the structure of the domain wall is interesting for applications, and it also provides a means to accurately determine fundamental material parameters, such as the size of the Dzyaloshinskii-Moriya interaction strength. The domain wall structure can be inferred using a variety of recent, novel experiments that measure the stray field above the magnetic wire, but the interpretation of these measurements requires an accurate theoretical method that relates the stray field to the magnetic structure. Here, various one-dimensional analytic methods for finding stray field are compared to MuMax simulations in order to determine if there exists an accurate analytic way to interpret a wide range of experiments. This has the advantage of being fast and simple compared to numerical simulations. Our analytic method relies on approximating the domain wall profile as a piecewise, linear function. It is shown to be accurate for parameters appropriate to CoPtCr nanowires that are 3 nm thick and 40–100 nm wide, and is expected to work broadly for nanowires that are thinner than the exchange length.

1. Introduction

In the last few years, experiments have measured the stray magnetic field produced by nano-magnets with new-found spatial resolution. Magnetic force microscopy, [1] nitrogen-vacancy nano-magnetometry [2–4] and micro-SQuID (superconducting quantum interference device) magnetometry [5] are providing new opportunities to measure stray magnetic fields with exquisite sensitivity and resolution. Precisely measuring the stray field of nanomagnets and thin films allows one to infer the underlying magnetization profile and therefore the precise strength of various important – and sometimes difficult to otherwise measure – material parameters. For example, Gross and coworkers were able to accurately determine the Dzyaloshinskii-Moriya interaction (DMI) in a micorometer-wide ribbon, by precisely measuring the angle of the magnetization in the center of a domain wall that was nucleated in the ribbon. [6]

In the step where experimental results are compared to theoretical predictions, in order to extract parameters such as the DMI strength, authors typically rely on micromagnetic solvers, such as OOMMF [7] or MuMax [8], which can be inefficient. Analytic methods have been used to *estimate* the stray field above nanomagnets but the models that have been used to date are approximate and consequently can introduce unnecessary sources of error into the analysis. In an ideal world, one would like an error-free, analytic expression as it is much quicker and easier to make predictions and compare to experimental results than running numerical simulations. Moreover, an analytical model provides a means to look at how the stray field varies explicitly as a function of various magnetic or geometric parameters.

Previously, we presented an extremely accurate, analytic calculation for the demagnetizing field *inside* a domain wall in a rectangular nanowire or ribbon. [9] That work predicted whether a Bloch or Néel wall will form in a particular magnetic material, as a function of the ribbon's aspect ratio. The results matched very well with those from experiments and micromagnetic simulations. A follow-up work extended the theory to treat domain walls with DMI present. [10] In this work, we use an analogous method to analytically find the stray field *above* the domain wall region.

We find that our analytic predictions agree very well with micromagnetic simulations done using MuMax. It is hoped that the developed expressions will be useful to scientists and engineers studying magnetic interactions in nanostructures, and making domain wall devices. In the supplemental material, we provide a user-friendly *Mathematica* code

* Corresponding author. Present address: School of Mathematical and Physical Sciences, The University of Newcastle, Callaghan, NSW 2308, Australia.
E-mail address: klivesey@uccs.edu (K.L. Livesey).

https://doi.org/10.1016/j.jmmm.2020.167164
Received 18 April 2020; Received in revised form 4 June 2020; Accepted 17 June 2020
Available online 29 June 2020

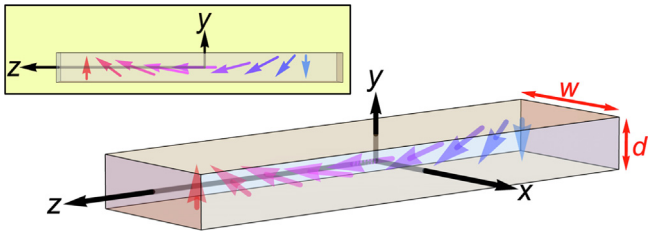

Fig. 1. The geometry of a rectangular nanowire with perpendicular magnetic anisotropy, width w and thickness d. The origin of the Cartesian coordinate system is at the center of the wire. The z direction is along the infinite wire's length. The wire is only a few nanometers thick in the y direction, but a 40–75 nm wide along the x direction. The muted arrows inside the wire represent the local magnetization direction in a Néel domain wall. The inset shows a side-on view.

that the reader can use to simply calculate the stray field anywhere in space, that is produced by a magnetic, rectangular nanoribbon containing a domain wall. Parameters may be chosen that correspond to any ferromagnetic material. DMI is not considered in this work as it greatly complicates domain wall profiles, [10,11] but may be included in the model in the future.

In Section 2 we describe the analytic method. More details and the long analytic expressions are provided in the Appendix. In Section III we will present results for some typical materials, with a comparison to results found using MuMax. Finally, in Section IV we present conclusions.

2. Analytic method

The geometry of the problem is shown in Fig. 1. An infinitely-long, rectangular, magnetic nanowire is extended in the z direction. The wire has width w in the x direction and thickness d in the y direction. We consider $d\sim$ 3 nm and $w\sim$ 40–75 nm. The model is also valid for larger w but the results are less interesting because the wire approaches the thin-film limit. The thickness d should be smaller than the exchange length so that the magnetization may be considered uniform in the y direction. The origin of the Cartesian coordinate system is located at the center of the wire. A domain wall centered at $z = 0$ is considered. We assume out-of-plane magnetic anisotropy so that the magnetization as $z \to -\infty$ $(+\infty)$ goes to $-M_s\hat{y}$ $(+M_s\hat{y})$, where M_s is the saturation magnetization.

We consider Bloch walls, where the magnetization inside the domain wall rotates in the $y-x$ plane (the magnetization in the domain wall center is along $\pm x$), plus Néel walls, where the magnetization rotates in the $y-z$ plane (the magnetization in the domain wall center is along $\pm z$). We can also use the developed expressions to find the stray field above a domain wall at some arbitrary angle in between, since this involves a linear superposition of the formulas. This is particularly important for DMI systems, and will be explained more later. DMI favors Néel walls of one chirality [12], so for low values of DMI "tilted" domain walls may form, that are somewhere between Bloch and Néel wall types. [13–15,10] In other words, the magnetization at the center of these walls points at an angle between the x and z axes.

The stray magnetic field is found by solving Maxwell's equations with a Green's function method. One wishes to solve $\nabla\cdot\vec{B} = 0 \Rightarrow \nabla\cdot\vec{H} = -\nabla\cdot\vec{M}$, in SI units. In addition, the stray field is represented by the gradient of a scalar magnetostatic potential, namely $\vec{H} = -\nabla U$, since $\nabla\times\vec{H} = 0$. The equation to solve therefore becomes $\nabla^2 U = \nabla\cdot\vec{M}$. The corresponding Green's function equation is the familiar Coulombic equation from electrostatics, namely $\nabla^2 G = \delta(\vec{r}-\vec{r}')$ with solution $G = 1/(4\pi|\vec{r}-\vec{r}'|)$. [16] One is then able to solve for the stray field of *any* magnetization distribution by integrating over the Green's function multiplied by the source terms [17]

$$\vec{H}(\vec{r}) = -\nabla\left(\int_V d^3\vec{r}'\,\frac{1}{4\pi|\vec{r}-\vec{r}'|}\nabla'\cdot\vec{M}(\vec{r}')\right). \tag{1}$$

The sources of stray field are gradients of the magnetization, $\nabla'\cdot\vec{M} = \partial_{x'}M_{x'} + \partial_{y'}M_{y'} + \partial_{z'}M_{z'}$. Note that both discontinuities in the magnetization (ie. at the edges of the nanowire) and smooth gradients in the magnetization (in the domain wall) produce stray field $\vec{H}$. In some instances, it is convenient to perform an integration by parts on Eq. (1) so that the Green's function G is differentiated twice. [18] Here, this is not necessary as the mathematics in fact may become more difficult. The various differentiations and integrations in Eq. (1) can all be done *analytically* if the magnetization profile $\vec{M}(\vec{r}')$ can be written as a linear piecewise function.

Before getting to the linear piecewise functions for $\vec{M}$, we state the one-dimensional (1D) domain wall profile for both a Bloch wall and a Néel wall. We note that for very narrow rectangular wires, the magnetization profile has been shown to not strictly have 1D dependence, because the magnetization curves at the edge of the wire. [19] However, the 1D domain wall profile works remarkably well for wires with width w = 40–75 nm for the parameters chosen here, and we discuss this below.

For a Bloch wall in our coordinate system, the 1D magnetization profile is:

$$\vec{M}(\vec{r}) = M_s\vec{m}^B(z)\left[\theta\left(x-\frac{w}{2}\right)-\theta\left(x+\frac{w}{2}\right)\right] \times\left[\theta\left(y-\frac{d}{2}\right)-\theta\left(y+\frac{d}{2}\right)\right], \tag{2}$$

where $\theta(x)$ is the Heaviside step function. The dimensionless vector $\vec{m}^B(z)$ describes the magnetization angle's dependence on position along the wire's length and is found by minimizing a 1D energy functional. [20,21] It is given by

$$m_x^B(z) = \pm\mathrm{sech}\left(\frac{z}{L_B}\right), \tag{3a}$$

$$m_y^B(z) = \tanh\left(\frac{z}{L_B}\right), \tag{3b}$$

$$m_z^B(z) = 0. \tag{3c}$$

The $\pm$ sign in Eq. (3)(a) shows that the domain wall can have one of two chiralities. The Bloch wall length L_B depends on the magnetic material parameters according to [9]

$$L_B = \sqrt{\frac{A}{K-\frac{1}{2}\mu_0 M_s^2(2N_y-1)}}, \tag{4}$$

where A is the exchange constant, K is the out-of-plane uniaxial anisotropy energy density, μ_0 is the permeability of free space, and N_y is a demagnetizing factor for a rectangular nanowire, given according to the aspect ratio by [22]

$$N_y(d,w) = \frac{2}{\pi}\arctan\left(\frac{w}{d}\right) + \frac{d}{\pi w}\ln(d/w) + \left(\frac{1-(d/w)^2}{2\pi d/w}\right)\ln(1+(d/w)^2). \tag{5}$$

For a Néel wall, the dimensionless vector $\vec{m}^B$ in Eq. (2) is replaced with $\vec{m}^N$, given by

$$m_x^N(z) = 0, \tag{6a}$$

$$m_y^N(z) = \tanh\left(\frac{z}{L_N}\right), \tag{6b}$$

$$m_z^N(z) = \pm\mathrm{sech}\left(\frac{z}{L_N}\right). \tag{6c}$$

The Néel wall length is [9]

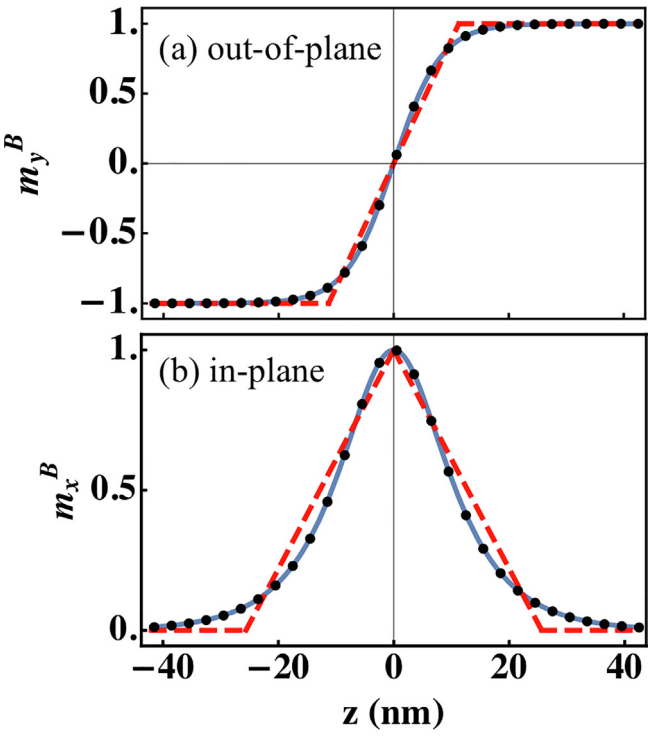

Fig. 2. The 1D magnetization profile of a Bloch domain wall in a rectangular nanowire, according to Eq. (3) (solid lines) and using MuMax simulations (black dots). A linear, piecewise approximation is also shown, as given by Eq. (8) (dashed lines). Panel (a) shows the out-of-plane magnetization component m_y^B as a function of position z, while panel (b) shows the in-plane m_x^B component. The parameters used are $d = 3$ nm, $w = 75$ nm (giving $N_y = 0.93$), $M_s = 3 \times 10^5$ A/m, $K = 2 \times 10^5$ J/m^3 and $A = 1 \times 10^{-11}$ J/m. The MuMax simulations split the nanowire into $1 \times 1 \times 3$ nm cells, with 3 nm being the total thickness of the wire.

$$L_N = \sqrt{\frac{A}{K - \frac{1}{2}\mu_0 M_s^2 N_y}}. \tag{7}$$

In fact, this approximation is a little naïve, as the volume demagnetization contribution of the Néel wall is not included in the estimate for L_N. [9,23] But we will show that this estimate provides satisfactory results.

We note that rather than using hyperbolic functions for the magnetization profile, a Lorentzian profile can be used instead, which has been done for Néel walls in thin films. [24,25] The hyperbolic functions are exact solutions for domain walls in thin films, and they have an extremely close match with our MuMax results for nanowires (to be shown in Fig. 2).

The linear piecewise approximation for the Bloch wall, also a 1D approximation, is denoted $\vec{a}^B(z) \sim \vec{m}^B(z)$ and has non-zero components [9]

$$a_x^B(z) = \begin{cases} \frac{z}{b_{Bx}} + 1, & -b_{Bx} < z < 0, \\ -\frac{z}{b_{Bx}} + 1, & 0 < z < b_{Bx} \\ 0, & \text{elsewhere} \end{cases}, \tag{8a}$$

$$a_y^B(z) = \begin{cases} -1, & z < -b_{By} \\ \frac{z}{b_{By}}, & -b_{By} < z < b_{By}. \\ +1, & b_{By} < z \end{cases} \tag{8b}$$

Here, the domain wall length parameters are given in terms of the Bloch wall width L_B according to

$$b_{Bx} = \pi L_B, \tag{9a}$$

$$b_{By} = \ln(4) L_B. \tag{9b}$$

These values give the best fit of the linear piecewise approximations to the smooth domain wall profiles. Fig. 2 shows the smooth Bloch domain profile given in Eq. (3) (solid lines), in comparison to the linear piecewise function given in Eq. (8) (dashed lines). In this figure, and all those that follow, the material parameters are appropriate for CoPtCr and follow Ref. [26]. These parameters are given in the figure caption. Panel (a) shows the out-of-plane magnetization and panel (b) shows the in-plane magnetization. Also drawn on both panels is the domain wall profile calculated using MuMax micromagnetic simulations (black dots). The magnetization is shown at the center of the nanowire and agrees exceptionally well with the 1D analytic expressions (solid lines). We note that at the edge of the stripe, the magnetization differs slightly from that in the center, [6] but the difference is under 2% for the parameters used here.

Similar to the Bloch wall, the linear piecewise approximation for the Néel wall is denoted $\vec{a}^N(z) \sim \vec{m}^N(z)$ and has non-zero components [9]

$$a_z^N(z) = \begin{cases} \frac{z}{b_{Nz}} + 1, & -b_{Nz} < z < 0, \\ -\frac{z}{b_{Nz}} + 1, & 0 < z < b_{Nz} \\ 0, & \text{elsewhere} \end{cases}, \tag{10a}$$

$$a_y^N(z) = \begin{cases} -1, & z < -b_{Ny} \\ \frac{z}{b_{Ny}}, & -b_{Ny} < z < b_{Ny}. \\ +1, & b_{Ny} < z \end{cases} \tag{10b}$$

Here, the domain wall length parameters are given in terms of the Néel wall width L_N in Eq. (7) according to

$$b_{Nx} = \pi L_N, \tag{11a}$$

$$b_{Ny} = \ln(4) L_N. \tag{11b}$$

Note that the same parameters will be used for the Néel wall as for the Bloch wall to plot the stray field components. The only difference is that the magnetic nanowire width $w = 40$ nm for the Néel wall and is $w = 75$ nm for the Bloch wall. This change of width causes the equilibrium domain wall type to switch. [9]

As with the Bloch wall, we have confirmed that the analytic solution matches within 1% with the results of a MuMax simulation (details of simulations are at the end of this section). The variation in the magnetization values in the center of the nanowire, compared to at an edge, is less than 1% for these parameters, supporting the use of a 1D analytic model.

To arrive at analytic expressions for the stray field in all space $\vec{H}(\vec{r})$, one must substitute Eq. (8) or Eq. (10) (the linear piecewise magnetization profiles), into Eq. (2), which is then in turn substituted into Eq. (1). This sounds very simple, but the various integrations and differentiations make the task very lengthy. Here we quote the results in the Appendix. Also included as a Supplemental Information file is a *Mathematica* notebook so that the reader may input magnetic parameters and in a matter of seconds calculate stray fields for any nanowire of interest, and fit to experimental measurements of stray magnetic fields.

We note that by using the smooth 1D hyperbolic magnetization profiles, given in Eq. (3) for the Bloch wall and in Eq. (5) for the Néel wall, one is able to do all the steps to find $\vec{H}(\vec{r})$ analytically, except for a final integration over z'. However, this integration over z' can be done numerically and is relatively quick. Thus, the results for a **linear, piecewise magnetization profile ("1D linear" as shorthand)** can be compare to those from the **1D smooth magnetization profile ("1D numerical")**, as a preliminary check of the results.

To test that the analytic expressions are accurate, their results are also compared to **MuMax micromagnetic simulations ("MuMax")**. These simulations involve splitting the magnetic nanowire into

elements that are 1 nm in width and length, and 3 nm thick (the total thickness of the nanowire). In other words, the nanowire is one micromagnetic cell thick. A nanowire that is 2 μm long is considered, which is sufficiently long so that the ends of the wire do not affect the stray magnetic field above the domain wall in the wire center. The magnetization is allowed to relax and then the total stray field is constructed by treating each micromagnetic element as a single magnetic dipole moment, and then summing up the dipolar fields from each one.

3. Results

As mentioned earlier, the parameters used throughout are taken from Ref. [26] and are appropriate for CoPtCr. Namely, they are thickness $d = 3$ nm, magnetization $M_s = 3 \times 10^5$ A/m, anisotropy $K = 2 \times 10^5$ J/m^3 and exchange $A = 1 \times 10^{-11}$ J/m. The width of the nanowire may be varied. Our previous 1D analytic model predicted that for a nanowire width of $w \leqslant 55$ nm, a Néel wall is energetically favorable, while for larger widths a Bloch wall is favored. [9] Note that for all widths used, the domain wall length L_B or L_N is roughly 8 nm for these parameters.

To test the analytic expressions for the stray field given in the Appendix, we first plot the three different components of the stray field at chosen positions above the nanowire ($y > 1.5$ nm), as a function of z along the wire's long axis. Then the determination of whether a wall is of Bloch or Néel type will be discussed.

In all of the plots that follow, the plot labels follow the same convention. The lines are the results from the 1D linear, analytic method. The square points show some results from doing a 1D numerical integration of the hyperbolic domain wall profiles. Finally, black dots show the profiles obtained from MuMax simulations. Few points are shown so as to not clutter the plots, since three methods of calculation are compared.

In most plots that follow, the stray field is calculated at three heights above the nanowire's center: $y = 30$ (solid, blue line), 60 (dashed, yellow line) and 120 nm (dashed, green line). Note that these distances are quoted from the origin at the center of the 3-nm thick wire, which places them at heights 28.5 nm, 58.5 nm and 118.5 nm above the top surface of the wire. Plot legends show exactly which line corresponds to 1D linear results at which height y.

3.1. H_x component

The component of the stray field that is in-plane and in the direction of the nanowire's width is examined first. Directly above the center of the nanowire ($x = 0$) the domains contribute nothing to this component of the stray field, so for this reason we choose to look at the behavior near the edge of the nanowire. Results are shown in Fig. 3(a) for H_x as a function of position z for a Bloch wall in a wire of width $w = 75$ nm, at $x = 37$ nm from the center, and at various heights y.

On first inspection, all three methods of calculation seem to agree very well, justifying the use of the analytic expressions. However, in Fig. 3(b) the analytic results are subtracted from the MuMax results and one sees that these differ at the center of the domain wall, up to 0.2 kA/m for the smallest height of just $y = 30$ nm. Moreover, the MuMax results have a stray field that passes through zero at $z > 0$, rather than closer to $z = 0$ as the 1D models predict due to symmetry. In fact, above the opposite edge of the nanowire ($x = -37$ nm, rather than $+37$ nm) the asymmetry seen in Fig. 3(b) is flipped about $z = 0$. These facts can be attributed to small variations in the magnetization profile across the width of the nanowire (x direction) that were discussed in Section 2 and were pointed out in Ref. [19]. MuMax data shows that the magnetization components differs by 2% or less at the edge of the wire compared to in the center ($x = 0$) but this small difference adds up when calculating the stray field from the entire structure. The difference becomes smaller at large distances from the center of the domain wall. An "S-shaped" domain wall forms [19] with very small in-plane M_z components ($|M_z/M_s| < 7 \times 10^{-3}$), so as to minimize the stray field energy of the Bloch wall in a nanowire with finite width. Interestingly, the other stray field components H_y and H_z seem less sensitive to these small magnetization variations in the x direction. Note that we have checked that the positions of the domain walls for the various calculation methods do in fact line up, and this is not a result of one domain wall being shifted along z compared to another. We also checked that the MuMax simulations were converged.

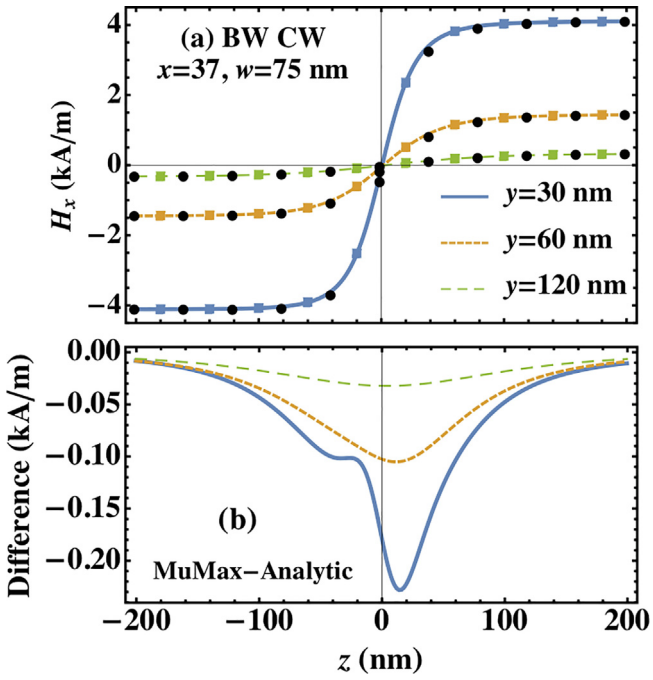

Fig. 3. (a) The stray field component H_x as a function of position z along the long axis of the wire. A Bloch wall with clockwise rotation is centered at $z = 0$ in a wire with $w = 75$ nm. The stray field is found above the wire's edge, at $x = 37$ nm. The lines are the 1D linear (analytic) results, the squares are the 1D numerical integration results, and the black dots are the MuMax simulations. (b) The difference between the MuMax results and the 1D linear, analytic results for H_x.

The analytic expression for the stray field component H_x can be simplified dramatically by assuming (incorrectly) that the domain wall length $L_B \to 0$. This far simpler result – which is given along with the full expressions in the Appendix – has very little error, compared to considering the full structure of the domain wall, as long as the height above the nanowire z is larger than the domain wall length L_B. For example, if $y = 5$ nm, one sees up to 50% error in the stray field near the domain wall region. But if $y = 15$ nm, the difference is a few percent. Again, this is in contrast to the other components (H_y and H_z) where ignoring the domain wall region leads to large errors, as will be discussed below.

3.2. H_y component

The out-of-plane stray field has a dominant contribution from the domains, reaching constant values above the domain regions for $|z| \gg L_{N/B}$. However, the wall region also contributes importantly near $z = 0$. Results for H_y are presented as a function of position z along the wire, at a position that is off a central axis of symmetry (ie. $y \neq 0$ and $x \neq 0$). This is so the differences between the Bloch and Néel wall's stray field can be seen clearly. Note that for precisely $x = 0$ the Bloch domain wall region does not contribute to H_y due to symmetry.

First, in Fig. 4, the out-of-plane component of the stray field near a $w = 40$ nm wire containing a Néel wall (NW) is shown at various heights for $x = 19.5$ nm (above the wire's edge), as a function of z. In

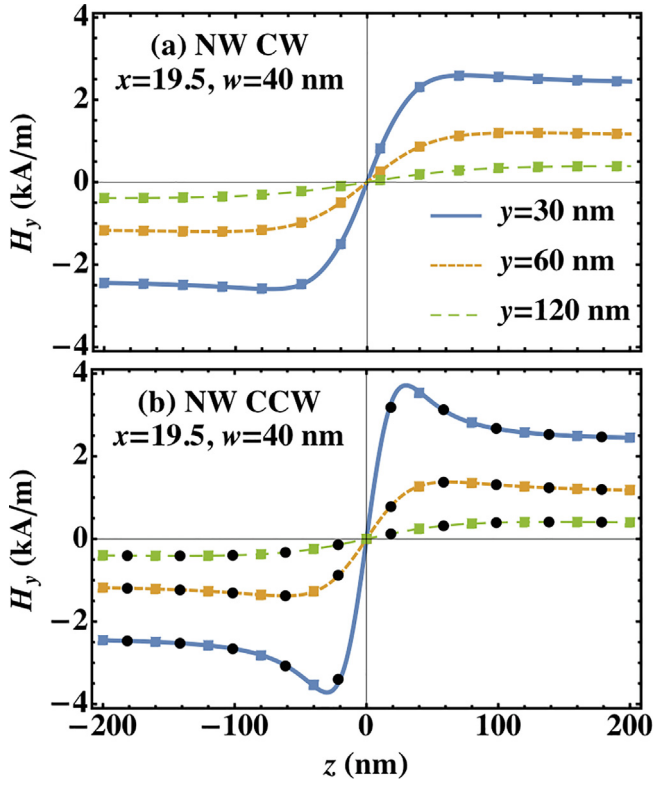

Fig. 4. The stray field component H_y as a function of position z along the long axis of the wire, for Néel walls with (a) CW and (b) CCW rotation, centered at $z = 0$ in a wire with $w = 40$ nm. Again, the lines are the 1D linear (analytic) results, the squares are the 1D numerical integration results, and the black dots are the MuMax simulations.

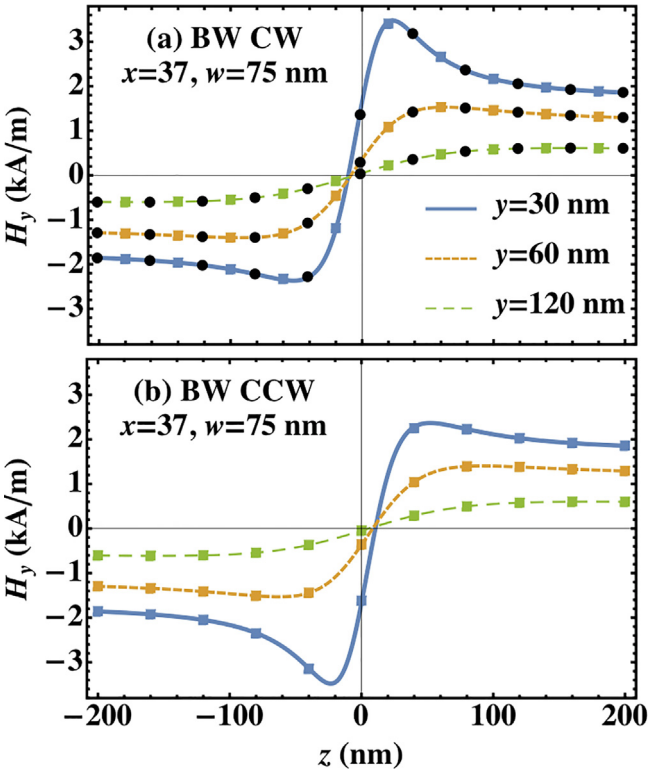

Fig. 5. The same as for Fig. 4, but for Bloch walls with (a) CW and (b) CCW rotation, centered at $z = 0$ in a wire with $w = 75$ nm.

panel (a), the results for a Néel wall with clockwise chirality (CW) are shown, while in panel (b) the results with counter-clockwise (CCW) chirality are shown. In panel (b) only, black dots indicate the results from MuMax. In all cases, the three calculation methods agree very well, showing that the 1D linear approximation yielding analytic results is a robust way to calculate the stray fields. Notice that the stray field magnitude decreases rapidly with increasing height above the wire.

Comparing the two panels in Fig. 4, one sees a larger magnitude "shoulder" in the stray field at the edges of the domain wall region for the CCW wall at $y = 30$ nm (panel (b), solid line) compared to the CW wall (panel (a)). This shoulder represents an increase in H_y of around 30% at $z = \pm 30$ nm. This is because the contribution to the out-of-plane stray field has a large contribution from the domain wall for the CCW rotation, which constructively adds with the domain contribution at both sides of the domain wall. For the opposite CW rotation (panel (a)), the domain wall contribution instead subtracts from the domain contribution. Above the domains, ($z \to \pm\infty$) the H_y magnitude approaches a constant value, which is the same in both panels.

Fig. 5 is very similar to Fig. 4 except that it shows results for Bloch walls with (a) CW and (b) CCW rotation. The out-of-plane component of the stray field near a $w = 75$ nm wire is shown at $x = 37$ nm, as a function of z. Three heights, $y = 30$, 60 and 120 nm, are again shown. The difference between all three methods – in all cases considered, both Bloch and Néel walls – is less than 0.02 kA/m (less than 1%).

Note that the limiting values of H_y out in the domains are different in Fig. 5 and 4 because the nanowires have different widths and the stray field is being probed at a different lateral position x. The stray field profile's shape in the domain wall region is also very different between the Bloch and Néel walls; namely, the Bloch wall has an asymmetric H_y profile about $z = 0$ (one of the shoulders is bigger than the other) while for the Néel wall it is symmetric and purely odd. In Fig. 5 the stray field is asymmetric near $z = 0$ (the center of the domain wall) because the domain wall contribution to the out-of-plane stray field from the Bloch wall (with moment along $\hat{x}$) is even, while the domain contribution is odd due to its curling nature about the origin. This results in the skewed plot for H_y. Note that this skew reverses its direction when the domain wall chirality is reversed (compare panels (a) and (b)). The skew vanishes at exactly $x = 0$ (results not shown) as directly above the center of the wire, the domain wall region contributes nothing to H_y because its dipolar field is purely parallel to $\pm\hat{x}$.

We mentioned earlier that the domain wall region contributes negligibly to H_x, as long as $y > 5$ nm. It is the domains that dominate the result. In contrast, for H_y the domain wall region is important for even relatively large heights above the nanowire, say $y = 50$ nm, as is evidenced by the asymmetry in Fig. 5 due to the domain wall's moment. Therefore, although letting the domain wall width vanish results in a vastly simplified expression for H_y (see Appendix) it gives spurious results (out by over 1 kA/m) in regions of interest.

Our results were also compared to approximate expressions given in Ref. [3], for Bloch and Néel walls of finite width, but in a thin-film material where $w \to \infty$. We note that their expression for the out-of-plane component of the stray field decays as $1/z$ away from the domain wall, which is not the behavior seen here where the stray field saturates. Therefore, a numerical comparison is not presented. In Ref. [3], the approximate expressions are used to motivate and understand the experiment, and micromagnetics is used to actually interpret the experimental results. Here, we provide a route to use analytic expressions to do both.

3.3. H_z component

Consider now the stray field component along the z direction (in-plane, along the wire's axis). The case of $w = 75$ nm (Bloch wall) is considered, and the resulting H_z component is plotted as a function of position z in Fig. 6. Positions directly above the center of the wire

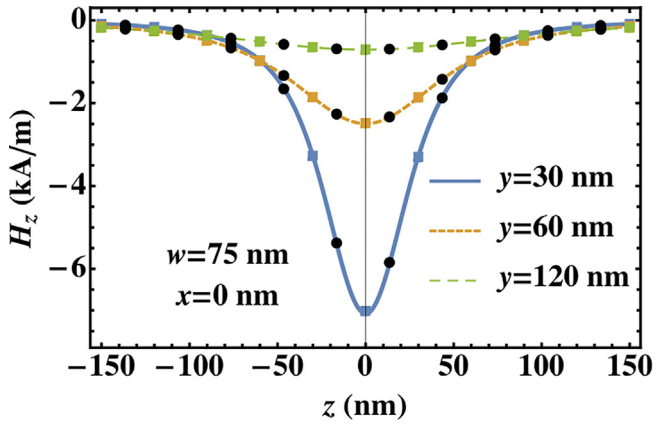

Fig. 6. The in-plane H_z component of the stray field for a Bloch wall, as a function of position z along the wire. The nanowire is 75 nm wide and the stray field is measured directly above its center ($x = 0$) at three different heights. The lines are the 1D linear (analytic) results, the squares are the 1D numerical integration results, and the black dots are the MuMax simulation results.

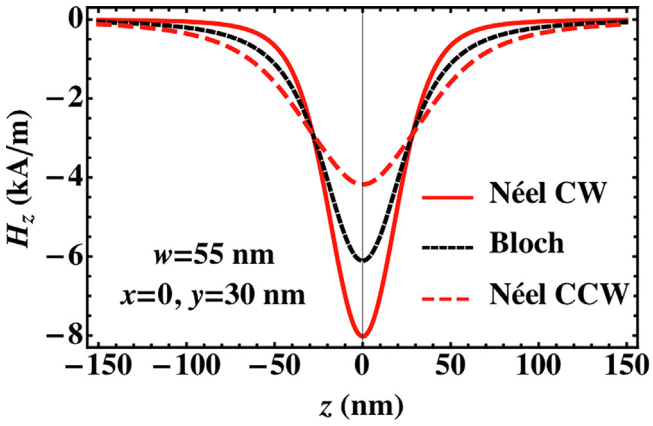

Fig. 7. The H_z component of the stray field directly above the central axis of a 55 nm-wide nanowire ($x = 0$, $y = 30$ nm). The 1D linear (analytic) results for a Néel wall (CW and CCW rotation) and a Bloch wall are shown.

($x = 0$) are taken at three different heights. There is a peak in the field component directly above the center of the domain wall, due purely to the stray field contribution from the domains. The moment of a Bloch domain wall is along the $\pm\,\hat{x}$ direction, so it contributes no stray field at this precise location ($x = z = 0$).

Once again, all three methods of calculation agree well. The difference between the 1D linear, analytic method and the MuMax results is less than 1% everywhere. The difference between the 1D numerical integration and the MuMax results is less than 0.1% everywhere. When the domain wall region is ignored in the 1D analytic method, then a very simple expression exists for H_z (see Appendix) but it produces a result that is 0.44 kA/m too large in magnitude in the center of the domain wall region ($z = 0$).

Fig. 6 is for $x = 0$, above the central axis of the nanowire. If one moves to above the edge of the nanowire, say $x = 37$ nm as considered when discussing H_y, then the Bloch domain wall region does influence H_z. Its effect is to make H_z asymmetric about $z = 0$ (the peak shifts either left or right, results not shown) because the wall's contribution to the stray field is odd while the domains' contribution is even. Once again, all three methods of calculation agree within 1%. This time, ignoring the domain wall's width in an analytic simplification leads to a serious problem as the asymmetry about z cannot be recovered without the domain wall contribution.

3.4. Determining Bloch from Néel walls

The results above all show that the 1D linear approximation works to calculate complicated magnetic stray fields quickly and accurately. Below we describe some additional results, which show the utility of this method for interpreting experiments. Tetienne *et al.* [3] were able to determine domain wall types (Bloch versus Néel or something in between) by measuring the stray field above a nanowire. This relied on a complicated calibration of the nitrogen-vacancy experiment, using micromagnetic simulations. The same analysis can be performed more rapidly and easily using analytic expressions, plus more insight can be gained on the physical contributions.

Consider, for example, a nanowire width $w = 55$ nm, where both Bloch and Néel walls are predicted to be stable for the parameters used throughout this work. [9] In Fig. 7 the H_z component of the stray field is plotted versus position z for a Bloch wall (black line) and Néel walls with opposite chirality, namely clockwise (CW, solid, red line) and counterclockwise (CCW, dashed, red line). The stray field is calculated above the center of the wire at $x = 0$, $y = 30$ nm. In other words, a line parallel to the z axis, that is 28.5 nm above the top surface of the nanowire, is considered. One sees that the magnitude of the stray field component varies by 50% in the center of the domain wall, depending on the domain wall type, as has been noted before using approximate stray field expressions. [3] Note that the stray field curls from the up domain ($z > 0$) to the down domain ($z < 0$) creating a H_z component of the stray field that is negative above the wire. For the two Néel wall chiralities, the domain wall region contributes to H_z in such a way as to either enhance (CCW) or diminish (CW) the stray field strength (red lines). As mentioned earlier when discussing Fig. 6, at precisely $x = 0$ the Bloch domain wall region does not contribute to H_z (only the domains contribute) so the result for the Bloch wall lies between the two Néel wall lines (black line).

The introduction of Dzyaloshinskii-Moriya interaction (DMI) can move the Bloch/Néel transition to larger wire widths, since DMI favors the Néel wall rotation. [10] In other words, the threshold width of 55 nm discussed earlier may become much larger. In fact, a domain wall that is neither a Bloch nor a Néel wall may form for moderate values of DMI. In other words, the magnetization in the center of the wall does not point along x (Bloch) or along $\pm\,z$ (Néel) but is instead at some intermediate angle. The measurement of stray fields can therefore be used to infer DMI strength or the effective magnetic width of nanostructures since H_z will have a profile between the two red lines drawn in Fig. 7.

4. Conclusions

The stray field from a rectangular, magnetic nanowire containing a domain wall is calculated a variety of ways. The results indicate that the 1D linear approximation for the domain wall profile leads to analytic expressions for the stray field that are accurate to within 1% of MuMax simulations in most cases of interest. For the parameters used here, appropriate for CoPtCr, the H_y and H_z components of the stray field are within 1% of the MuMax results for a vast range of positions around the domain wall. The H_x component has an error of 0.2 kA/m, 30 nm above the domain wall's center and at the edge of the nanowire, due to small variations in the domain wall profile across the nanowire width (x direction).

The advantage of the 1D linear expressions for the stray field is that they are computationally cheap and also allows one to look at how the fields depend on various parameters such as nanowire dimensions. In fact, a whole stray field vector plot can be generated in a few seconds, allowing experimentalists to quickly and accurately compare their results to theory.

Although a single domain wall in an infinitely-long nanowire has been considered here, the general idea to linearize magnetization profiles in order to find stray fields analytically can be used to study other

systems, for example, wires or thin films with multiple domain walls present, or even skyrmions where cylindrical rather than Cartesian coordinate systems can be used.

Declaration of Competing Interest

The authors declare that they have no known competing financial interests or personal relationships that could have appeared to influence the work reported in this paper.

Acknowledgments

Dr. J.-V. Kim is thanked for answering questions on previous stray field calculations. A.R.S. acknowledges support from the UCCS Undergraduate Research Academy. A.R.S. and K.L.L. acknowledge funding from NSF DMR-1808412, and C.Q.F. and K.S.B. acknowledge funding from NSF DMR-1709525.

Appendix A. Analytic expressions for the stray field

Here, the analytic, 1D expressions we developed for the stray field of Bloch and Néel walls in nanowires are provided. To help the reader, we summarize the key equations below that are needed to produce the stray field. For a Bloch wall, the stray field components are given by.

- H_x: Eqs. (A.2), (A.4) and (A.8),
- H_y: Eqs. (A.10), (A.12) and (A.15),
- H_z: Eqs. (A.17), (A.19), (A.21) and (A.22).

For a Néel wall, the stray field components are given by

- H_x: Eqs. (A.2), (A.6) and (A.8),
- H_y: Eqs. (A.10), (A.13), (A.14) and (A.15),
- H_z: Eqs. (A.17), (A.20), (A.21) and (A.22).

In the following, some shorthand notations will be helpful to reduce the size of the expressions. They are $X = x - x'$, $Y = y - y'$, $Z = z - z'$, $R = |\vec{r} - \vec{r}'| = \sqrt{X^2 + Y^2 + Z^2}$, arctanh = atanh, and arctan = atan. Also note that the domain wall region's length is given by b_x, b_y and b_z as shorthand, for the three different magnetization components. These values are determined from material parameters and nanowire dimensions and are given for Bloch walls in Eqs. (4), (9), and for Néel walls in Eqs. (7), (11) of the main text. Recall that the reason the domain wall region has a different effective length for the different magnetization components is to ensure that the approximate, linear-piecewise magnetization profiles have best fit with the hyperbolic, exact profiles (see Fig. 2).

Note that some terms in the expressions that follow are complex, however the total expressions for the stray field components are all purely real.

A.1. H_x component

We start with the stray field component $H_x(\vec{r})$. It is

$$H_x(\vec{r}) = -\partial_x \int_V d^3\vec{r}' \frac{1}{4\pi|\vec{r} - \vec{r}'|} \nabla' \cdot \vec{M}(\vec{r}'). \tag{A.1}$$

We can split Eq. (A.1) into three dimensionless contributions, namely

$$4\pi \frac{H_x(\vec{r})}{M_s} \equiv h_x(\vec{r}) = h_{xx} + h_{xy} + h_{xz}, \tag{A.2}$$

where each piece is defined as

$$h_{x\alpha} = -\partial_x \int_V d^3\vec{r}' \frac{1}{M_s R} \partial_{\alpha'} \vec{M}_{\alpha'}(\vec{r}'), \quad \alpha = x, y, z. \tag{A.3}$$

For the Néel wall $h_{xx} = 0$ because there is no magnetization component along x, but for the Bloch wall it is

$$h_{xx} = \mathscr{C} \left[\left[\left[\frac{X}{b_x} \ln(Y + R) + \left(1 + \frac{z}{b_x}\right) \left\{ \operatorname{atan}\left(-\frac{Z}{X}\right) + \operatorname{atan}\left(\frac{YZ}{XR}\right) \right\} \right]_{-\frac{w}{2}}^{\frac{w}{2}} \right]_{-\frac{d}{2}}^{\frac{d}{2}} \right]_{-b_x}^{0} \tag{A.4}$$

$$+ \mathscr{C} \left[\left[\left[-\frac{X}{b_x} \ln(Y + R) + \left(1 - \frac{z}{b_x}\right) \left\{ \operatorname{atan}\left(-\frac{Z}{X}\right) + \operatorname{atan}\left(\frac{YZ}{XR}\right) \right\} \right]_{-\frac{w}{2}}^{\frac{w}{2}} \right]_{-\frac{d}{2}}^{\frac{d}{2}} \right]_{0}^{b_x}$$

where the square parentheses indicate that the expression needs to be evaluated at $x' = w/2$ and $x' = -w/2$, at $y' = d/2$ and $y' = -d/2$, and at the ends and middle of the domain wall region, namely $z' = 0$ and $z' = \pm b_x = \pm b_{Bx}$. Note that $\mathscr{C}$ is a chirality factor given by

$$\mathscr{C} = \begin{cases} +1, & \text{Bloch wall moment along} +\hat{x} \ \text{(CW)}, \\ -1, & \text{Bloch wall moment along} -\hat{x} \ \text{(CCW)}. \end{cases} \tag{A.5}$$

Similarly, for the Bloch wall $h_{xz} = 0$, but for the Néel wall it is

$$h_{xz} = \mathscr{C}\left[\left[\left[-\frac{X}{b_z}\text{atan}\left(\frac{YZ}{XR}\right) - \frac{Y}{b_z}\ln(-Z+R) + (z+b_z)\text{atanh}\left(\frac{R}{Y}\right)\right]_{-\frac{w}{2}}^{\frac{w}{2}}\right]_{-\frac{d}{2}}^{\frac{d}{2}}\right]_{-b_z}^{0} \tag{A.6}$$

$$+ \mathscr{C}\left[\left[\left[\frac{X}{b_z}\text{atan}\left(\frac{YZ}{XR}\right) + \frac{Y}{b_z}\ln(-Z+R) + (-z+b_z)\text{atanh}\left(\frac{R}{Y}\right)\right]_{-\frac{w}{2}}^{\frac{w}{2}}\right]_{-\frac{d}{2}}^{\frac{d}{2}}\right]_{0}^{b_z},$$

where again these expressions are evaluated at the edges of the magnetic nanowire, at the center of the domain wall ($z' = 0$) and at the domain wall edges ($z' = \pm b_z = \pm b_{Nz}$). Again, $\mathscr{C}$ is a chirality factor given by

$$\mathscr{C} = \begin{cases} +1, & \text{Neel wall moment along} +\hat{z} \ \text{(CW)}, \\ -1, & \text{Neel wall moment along} -\hat{z} \ \text{(CCW)} \end{cases}. \tag{A.7}$$

The final piece of $H_x(\vec{r})$ is common to both the Bloch and Néel walls, since both have out-of-plane magnetization components. It is

$$h_{xy} = \frac{1}{b_y}\left[\left[\left[R + z\ln(-Z+R)\right]_{-\frac{w}{2}}^{\frac{w}{2}}\right]_{-\frac{d}{2}}^{\frac{d}{2}}\right]_{-b_y}^{b_y} \tag{A.8}$$

$$- \left[\left[\text{atanh}\left(-\frac{Z}{R}\right)\right]_{-\frac{w}{2}}^{\frac{w}{2}}\right]_{-\frac{d}{2}}^{\frac{d}{2}}\Bigg|_{z'=-b_y} - \left[\left[\text{atanh}\left(-\frac{Z}{R}\right)\right]_{-\frac{w}{2}}^{\frac{w}{2}}\right]_{-\frac{d}{2}}^{\frac{d}{2}}\Bigg|_{z'=b_y},$$

where the domain wall region has length b_y that is b_{By} for the Bloch wall and is b_{Ny} for the Néel wall.

When the domain wall length is assumed to vanish, then h_{xy} is the only one of the three terms in H_x to survive and one arrives at a simple formula, that has been used by others, namely

$$H_x(\vec{r}) \sim -\frac{M_s}{2\pi}\left[\left[\text{atanh}\left(\frac{-z}{|\vec{r}-\vec{r}'|}\right)\right]_{-\frac{w}{2}}^{\frac{w}{2}}\right]_{-\frac{d}{2}}^{\frac{d}{2}}. \tag{A.9}$$

The consequences of using this assumption are discussed in the main text.

A.2. H_y component

In analogous fashion to what was done to calculate $H_x(\vec{r})$, we can split $H_y(\vec{r})$ into three dimensionless contributions, namely

$$4\pi\frac{H_y(\vec{r})}{M_s} \equiv h_y(\vec{r}) = h_{yx} + h_{yy} + h_{yz}, \tag{A.10}$$

where each piece is defined as

$$h_{y\alpha} = -\partial_y \int_V d^3\vec{r}\,'\frac{1}{M_s R}\partial_{\alpha'}\vec{M}_{\alpha'}(\vec{r}\,'), \quad \alpha = x, y, z. \tag{A.11}$$

Then each of the three pieces can be found by differentiating and integrating in the most useful order.

The Bloch wall has non-zero h_{yx} given by

$$h_{yx} = \mathscr{C}\left[\left[\left[-\ln(Z+R) + \frac{R}{b_x} + \frac{z}{b_x}\ln(-Z+R)\right]_{-\frac{w}{2}}^{\frac{w}{2}}\right]_{-\frac{d}{2}}^{\frac{d}{2}}\right]_{-b_x}^{0} \tag{A.12}$$

$$+ \mathscr{C}\left[\left[\left[-\ln(Z+R) - \frac{R}{b_x} - \frac{z}{b_x}\ln(-Z+R)\right]_{-\frac{w}{2}}^{\frac{w}{2}}\right]_{-\frac{d}{2}}^{\frac{d}{2}}\right]_{0}^{b_x}.$$

The Néel wall has non-zero h_{yz} given by

$$h_{yz}=\mathscr{C}\left[\left[\left[\operatorname{atanh}\left(\frac{R}{X}\right)-\frac{1}{b_z}g(x,y,z,x',y',z')\right]_{-\frac{w}{2}}^{\frac{w}{2}}\right]_{-\frac{d}{2}}^{\frac{d}{2}}\right]_{-b_z}^{0} + \mathscr{C}\left[\left[\left[\operatorname{atanh}\left(\frac{R}{X}\right)+\frac{1}{b_z}g(x,y,z,x',y',z')\right]_{-\frac{w}{2}}^{\frac{w}{2}}\right]_{-\frac{d}{2}}^{\frac{d}{2}}\right]_{0}^{b_z}, \tag{A.13}$$

where the integrand piece g is defined as

$$g(x,y,z,x',y',z') = Y\ \operatorname{atan}\left(\frac{XZ}{YR}\right) - z\ \operatorname{atanh}\left(\frac{R}{X}\right) - X\ln(Z+R). \tag{A.14}$$

Both the Bloch and Néel walls have contribution h_{yy} given by

$$h_{yy} = \left[\left[\left[\frac{z}{b}\operatorname{atan}\left(\frac{XZ}{YR}\right)+\frac{Y}{b_y}\operatorname{atanh}\left(\frac{R}{X}\right)\right]_{-\frac{w}{2}}^{\frac{w}{2}}\right]_{-\frac{d}{2}}^{\frac{d}{2}}\right]_{-b_y}^{b_y} - \left[\left[\operatorname{atan}\left(\frac{XZ}{YR}\right)\right]_{-\frac{w}{2}}^{\frac{w}{2}}\right]_{-\frac{d}{2}}^{\frac{d}{2}}\Bigg|_{z'=-b_y} - \left[\left[\operatorname{atan}\left(\frac{XZ}{YR}\right)\right]_{-\frac{w}{2}}^{\frac{w}{2}}\right]_{-\frac{d}{2}}^{\frac{d}{2}}\Bigg|_{z'=b_y}. \tag{A.15}$$

Assuming that the domain wall has negligible width, then the total component H_y only has contribution from h_{yy} (the domains) and is given by

$$H_y(\vec{r})\sim -\frac{M_s}{2\pi}\left[\left[\operatorname{atan}\left(\frac{z(x-x')}{(y-y')|\vec{r}-\vec{r}'|}\right)\right]_{-\frac{w}{2}}^{\frac{w}{2}}\right]_{-\frac{d}{2}}^{\frac{d}{2}}. \tag{A.16}$$

Note that here $z'=0$ in the calculation of $|\vec{r}-\vec{r}'|$. In the main text, we explain how this is a poor approximation for H_y compared to using the full equations above.

A.3. H_z component

$H_z(\vec{r})$ is split into three dimensionless contributions, namely

$$4\pi\frac{H_z(\vec{r})}{M_s} \equiv h_z(\vec{r}) = h_{zx} + h_{zy} + h_{zz}, \tag{A.17}$$

where each piece is defined as

$$h_{z\alpha} = -\partial_z \int_V d^3\vec{r}'\frac{1}{M_s R}\partial_{\alpha'}\vec{M}_{\alpha'}(\vec{r}'), \quad \alpha = x,y,z. \tag{A.18}$$

Then each of the three pieces can be found by differentiating and integrating.

The Bloch wall has non-zero contribution h_{zx} given by

$$h_{zx}b_x=\mathscr{C}\left[\left[\left[\operatorname{sgn}(Y)\left\{-(b+z)\operatorname{atanh}\left(\frac{R}{|Y|}\right)+|X|\operatorname{atan}\left(\frac{|Y|Z}{|X|R}\right)\right\}-Y\ln(Z+R)\right]_{-\frac{w}{2}}^{\frac{w}{2}}\right]_{-\frac{d}{2}}^{\frac{d}{2}}\right]_{-b_x}^{0} + \mathscr{C}\left[\left[\left[-\operatorname{sgn}(Y)\left\{(b-z)\operatorname{atanh}\left(\frac{R}{|Y|}\right)+|X|\operatorname{atan}\left(\frac{|Y|Z}{|X|R}\right)\right\}+Y\ln(Z+R)\right]_{-\frac{w}{2}}^{\frac{w}{2}}\right]_{-\frac{d}{2}}^{\frac{d}{2}}\right]_{0}^{b_x}. \tag{A.19}$$

The Néel wall has non-zero contribution h_{zz} given by

$$h_{zz}b_z=-\mathscr{C}\left[\left[\left[y'+Z\operatorname{atan}\left(\frac{Y}{Z}\right)-Z\operatorname{atan}\left(\frac{XY}{ZR}\right)+Y\ln(X+R)+X\ln(Y+R)\right]_{-\frac{w}{2}}^{\frac{w}{2}}\right]_{-\frac{d}{2}}^{\frac{d}{2}}\right]_{-b_z}^{0} + \mathscr{C}\left[\left[\left[y'+Z\operatorname{atan}\left(\frac{Y}{Z}\right)-Z\operatorname{atan}\left(\frac{XY}{ZR}\right)+Y\ln(X+R)+X\ln(Y+R)\right]_{-\frac{w}{2}}^{\frac{w}{2}}\right]_{-\frac{d}{2}}^{\frac{d}{2}}\right]_{0}^{b_z}. \tag{A.20}$$

Both the Bloch and Néel walls have h_{zy} that has a contribution from the domains h_{zy}^{dom} and a contribution from the domain wall region h_{zy}^{DW}. In other

words, $h_{zy} = h_{zy}^{\mathrm{dom}} + h_{zy}^{\mathrm{DW}}$. Most notably, the Néel wall can have two possible chiralities (discussed in the main text) with one chirality reinforcing the stray field from the domains above the domain wall region, and the other chirality reducing the stray field magnitude there. The domain wall contribution is

$$h_{zy}^{\mathrm{DW}} b_z = \left[\left[\left[-z\mathrm{atanh}\left(\frac{R}{X}\right) + Y\mathrm{atan}\left(\frac{XZ}{YR}\right) - X\ln(Z+R)\right]_{-\frac{w}{2}}^{\frac{w}{2}}\right]_{-\frac{d}{2}}^{\frac{d}{2}}\right]_{-b_y}^{b_y} \tag{A.21}$$

and the domain contribution is

$$h_{zy}^{\mathrm{dom}} = \left[\left[\mathrm{atanh}\left(\frac{R}{X}\right)\right]_{-\frac{w}{2}}^{\frac{w}{2}}\right]_{-\frac{d}{2}}^{\frac{d}{2}}\Bigg|_{z'=-b_y} + \left[\left[\mathrm{atanh}\left(\frac{R}{X}\right)\right]_{-\frac{w}{2}}^{\frac{w}{2}}\right]_{-\frac{d}{2}}^{\frac{d}{2}}\Bigg|_{z'=b_y}. \tag{A.22}$$

Assuming that the domain wall has negligible width, then the total component H_z only has contribution from h_{zy} and is given by (with $z' = 0$)

$$H_z(\vec{r}) \sim -\frac{M_s}{2\pi}\left[\left[\mathrm{atan}\left(\frac{|\vec{r} - \vec{r}'|}{(x - x')}\right)\right]_{-\frac{w}{2}}^{\frac{w}{2}}\right]_{-\frac{d}{2}}^{\frac{d}{2}}. \tag{A.23}$$

Appendix B. Supplementary data

Supplementary data associated with this article can be found, in the online version, at https://doi.org/10.1016/j.jmmm.2020.167164.

References

[1] K.-H. Tu, S. Ojha, C.A. Ross, J. Phys. D: Appl. Phys. 51 (2018) 215002.
[2] L. Rondin, J.-P. Tetienne, T. Hingant, J.-F. Roch, P. Maletinsky, V. Jacques, Rep. Prog. Phys. 77 (2014) 056503.
[3] J.-P. Tetienne, T. Hingant, L. Martínez, S. Rohart, A. Thiaville, L.H. Diez, K. Garcia, J.-P. Adam, J.-V. Kim, J.-F. Roch, I. Miron, G. Gaudin, L. Vila, D. Ocker, D. Ravelsona, V. Jacques, Nat. Commun. 6 (2015) 6733.
[4] F. Casola, T. van der Sar, A. Yacoby, Nat. Rev. Mater. 3 (2018) 17088.
[5] D. Vasyukov, L. Ceccarelli, M. Wyss, B. Gross, A. Schwarb, A. Mehlin, N. Rossi, G. Tütüncüoglu, F. Heimbach, R. Zamani, A. Kovács, D. Grundler, M. Poggio, Nano Lett. 18 (2018) 964.
[6] I. Gross, L. Martínez, J.-P. Tetienne, T. Hingant, J.-F. Roch, K. Garcia, R. Soucaille, J. Adam, J.-V. Kim, S. Rohart, A. Thiaville, J. Torrejon, M. Hayashi, V. Jacques, Phys. Rev. B 94 (2016) 064413.
[7] M.J. Donahue, M. Donahue, OOMMF user's guide, version 1.0 (US Department of Commerce, National Institute of Standards and Technology (1999).
[8] A. Vansteenkiste, B. Van de Wiele, J. Magn. Magn. Mater. 323 (2011) 2585.
[9] M.D. DeJong, K.L. Livesey, Phys. Rev. B 92 (2015) 214420.
[10] M.D. DeJong, K.L. Livesey, Phys. Rev. B 95 (2017) 054424.
[11] C.B. Muratov, V.V. Slastikov, A.G. Kolesnikov, O.A. Tretiakov, Phys. Rev. B 96 (2017) 134417.
[12] M. Heide, G. Bihlmayer, S. Blügel, Phys. Rev. B 78 (2008) 140403.
[13] O.A. Tretiakov, A. Abanov, Phys. Rev. Lett. 105 (2010) 157201.
[14] A. Thiaville, S. Rohart, É. Jué, V. Cros, A. Fert, EPL (Europhysics Letters) 100 (2012) 57002.
[15] O. Boulle, S. Rohart, L. Buda-Prejbeanu, E. Jué, I. Miron, S. Pizzini, J. Vogel, G. Gaudin, A. Thiaville, Phys. Rev. Lett. 111 (2013) 217203.
[16] G. Rickayzen, Green's Functions and Condensed Matter (Dover, 2013) Chap. 1.
[17] J.D. Jackson, Classical Electrodynamics, third ed., John Wiley & Sons, 1999 p. 196.
[18] K.Y. Guslienko, A.N. Slavin, J. Magn. Magn. Mater. 323 (2011) 2418.
[19] B. Boehm, A. Bisig, A. Bischof, G. Stefanou, B. Hickey, R. Allenspach, Phys. Rev. B 95 (2017) 180406.
[20] H.-B. Braun, Phys. Rev. B 50 (1994) 16485.
[21] A. Hubert, R. Schäfer, Magnetic domains: the analysis of magnetic microstructures, Springer-Verlag, Berlin, 2008.
[22] W.F. Brown, Magnetostatic Principles in Ferromagnetism vol. 1, North-Holland Publishing Company, Amsterdam, 1962.
[23] A. Mougin, M. Cormier, J. Adam, P. Metaxas, J. Ferré, Europhys. Lett. 78 (2007) 57007.
[24] A. Aharoni, Introduction to the Theory of Ferromagnetism, Oxford University Press, Oxford, 2000.
[25] C.-Y. You, S.D. Bader, J. Appl. Phys. 92 (2002) 3886.
[26] E. Martinez, L. Torres, L. Lopez-Diaz, Phys. Rev. B 83 (2011) 174444.